

Photometric Confirmation of MACHO Large Magellanic Cloud Microlensing Events

David P. Bennett¹, Andrew C. Becker², and Austin Tomaney³

ABSTRACT

We present previously unpublished photometry of three Large Magellanic Cloud (LMC) microlensing events and show that the new photometry confirms the microlensing interpretation of these events. These events were discovered by the MACHO Project alert system and were also recovered by the analysis of the 5.7 year MACHO data set. This new photometry provides a substantial increase in the signal-to-noise ratio over the previously published photometry and in all three cases, the gravitational microlensing interpretation of these events is strengthened. The new data consist of MACHO-Global Microlensing Alert Network (GMAN) follow-up images from the CTIO 0.9 telescope plus difference imaging photometry of the original MACHO data from the 1.3m “Great Melbourne” telescope at Mt. Stromlo. We also combine microlensing light curve fitting with photometry from high resolution HST images of the source stars to provide further confirmation of these events and to show that the microlensing interpretation of event MACHO-LMC-23 is questionable. Finally, we compare our results with the analysis of Belokurov, Evans & Le Du who have attempted to classify candidate microlensing events with a neural network method, and we find that their results are contradicted by the new data and more powerful light curve fitting analysis for each of the four events considered in this paper. The failure of the Belokurov, Evans & Le Du method is likely to be due to their use of a set of insensitive statistics to feed their neural networks.

Subject headings: gravitational lensing, Galaxy: halo, Magellanic Clouds, dark matter

1. Introduction

The decade of the 1990s saw the development of gravitational microlensing as a new method to detect objects in the planet through stellar mass range through their gravitational effect on light rays from background stars (Alcock et al. 1993; Aubourg et al. 1993; Udalski et al. 1993). Applications of this method include such diverse topics as the search for baryonic dark matter in the Milky Way halo (Alcock et al. 1997b, 2000c; Lasserre et al. 2000; Afonso et al. 2003a), the discovery of planets orbiting distant stars

¹Department of Physics, University of Notre Dame, IN 46556, USA
Email: bennett@nd.edu

²Astronomy Department, University of Washington, Seattle, WA 98195, USA
Email: becker@astro.washington.edu

³Applied Biosystems, 850 Lincoln Centre Dr., Foster City, CA 94404, USA
Email: TomaneAB@appliedbiosystems.com

(Bond et al. 2004), limb darkening measurements of distant stars (Albrow et al. 1999), and obtaining high S/N spectra of distant stars that would otherwise be possible only with future extremely large telescopes (Lennon et al. 1996; Minniti et al. 1998).

The original proposal for this method was the suggestion by Paczyński (1986) to use microlensing to determine if the Milky Way’s dark halo is made up of brown dwarfs or jupiters. (Dark matter objects that can be detected via microlensing are often referred to as MAssive Compact Halo Object or MACHOs.) The MACHO and EROS groups have completed the microlensing survey proposed by Paczyński (1986), and their main result is the conclusion that the Milky Way’s dark halo is *not* dominated by objects with masses in the planet-stellar mass range (Alcock et al. 1998, 1997b, 2000c; Lasserre et al. 2000; Alcock et al. 2001a; Afonso et al. 2003a). Objects in the entire mass range, $10^{-7} - 30 M_{\odot}$ are excluded from dominating the Milky Way’s dark halo, with upper limits extending down to $< 5\%$ of the dark halo mass for sub-stellar mass objects. However, the MACHO Project (Alcock et al. 2000c) has found a microlensing signal above the expected background due to lensing by known stellar populations in the Milky Way and Large Magellanic Cloud (LMC). This signal has a microlensing optical depth equivalent to a dark halo with a MACHO fraction of about 20%, although the total mass could be somewhat smaller with if the MACHOs have a distribution that resembles a spheroid or a very thick disk rather than the dark halo (Gates & Gyuk 2001). Some of the first results from M31 microlensing observations appears to confirm this result (Uglesich et al. 2004; Calchi Novati et al. 2005). The timescale of the LMC microlensing events indicates a typical mass of $\sim 0.5M_{\odot}$, so the most plausible lens objects are white dwarfs, because main sequence stars of this mass would be much too bright to have previously escaped detection. However, there are a number of potential problems with the white dwarf explanation of this LMC microlensing excess (Torres, García-Berro, Burkert, & Isern 2002; Flynn, Holopainen, & Holmberg 2003; Brook, Kawata, & Gibson 2003; García-Berro, Torres, Isern, & Burkert 2004; Spagna, Carollo, Lattanzi, & Bucciarelli 2004). On the other hand, many of the constraints are evaded if most of the halo white dwarfs have Helium atmospheres. It might also be possible to explain the MACHO results with a population dominated by lower mass objects (Rahvar 2005).

The leading alternative explanation for the LMC microlensing excess is that the lens objects are ordinary stars associated with the LMC (Sahu 1994). However, standard models of the LMC predict that MACHO should have detected only 2-4 events from known stellar populations (Wu 1994; Alcock et al. 2000c), and there is a simple dynamical explanation for the small LMC self-lensing optical depth (Gould 1995b). On the other hand, the LMC is not an isolated galaxy and may have had significant dynamical disturbances from the Milky Way (Weinberg 2000; Evans & Kerins 2000), but current LMC models that include these effects still cannot account for the observed microlensing events (Gyuk, Dalal, & Griest 2000; Alves 2004; Mancini, Calchi Novati, Jetzer, & Scarpetta 2004; Nikolaev et al. 2004) because most of the events do not occur in the regions of the highest predicted LMC self-lensing rate.

The other logical possibility is that the background of microlensing events due to faint stars in the local Galactic disk could have been underestimated, but the lens stars for such events should be readily observed in both high resolution and IR observations as event MACHO-LMC-5 has demonstrated (Alcock et al. 2001d; Drake, Cook, & Keller 2004; Gould, Bennett, & Alves 2004; Nguyen et al. 2004) In fact, most candidate Milky Way disk events are readily identifiable through their anomalous unmagnified colors in the MACHO

data, and of the other published microlensing candidates, only MACHO-LMC-20 appears consistent with lensing by a low mass disk star. Thus, this possibility appears to be less likely than halo or LMC lenses.

Of course, all of this assumes that the MACHO LMC microlensing results are correct. The EROS collaboration has also monitored the LMC for microlensing events, but have detected fewer events than MACHO and reported an upper limit on the microlensing optical depth that is only barely consistent with the MACHO detection (Lasserre et al. 2000). A similar near-discrepancy holds for microlensing towards the Galactic bulge, where MACHO also measured a higher microlensing optical depth (Popowski et al. 2004) than EROS (Afonso et al. 2003b) In this case, the MACHO result is clearly favored as it is more consistent with separate measurements by OGLE (Udalski et al. 1994a) and MOA (Sumi et al. 2003), as well as a completely independent measurement by MACHO (Alcock et al. 2000b).

1.1. Event Selection by Neural Networks

The difficulty with interpreting the LMC results combined with the near-discrepancy between the MACHO and EROS results, has led Belokurov, Evans & Le Du (2003, 2004) (hereafter BEL) to attempt to develop an independent microlensing event selection method for the MACHO data set. In an attempt to improve upon the MACHO event selection method, BEL have introduced a method using neural networks instead of the series of simple cuts on statistics used by MACHO. This method seemed promising because neural networks should be able to find a set of event selection cuts that are more efficient at identifying microlensing events than can be easily obtained by more traditional trial-and-error methods. However, a major drawback of neural networks is their “black box” nature: it is not obvious exactly why the neural network might make its event classification decisions. Thus, a neural network could mysteriously fail to identify real microlensing events if there was some subtle difference between the real data and the example events used in the training set for the neural network, and it would be difficult to find such an error. This is the reason that neural networks were not used in the MACHO analysis, and it appears to have led BEL and Evans & Belokurov (2004) to over-interpret their results.

In fact, the specific neural network implementation of BEL has a number of serious flaws. Ideally, one would simply feed the raw time series photometry and error estimates into the neural network, and let the neural network sort out how to find microlensing events. With hundreds or thousands of input values, such a neural network would be far too slow to be practical. A practical neural network implementation can be obtained if we reduce the raw light curve data to a much smaller number of statistics that can be calculated from the raw data. The choice of these statistics is, of course, critical to the success of the neural network classification method, and this is where the method of BEL appears to fail. BEL select a set of statistics that are based upon auto- and cross-correlation functions of the light curve data, with the time series treated as if they were sampled uniformly in time (which they certainly are not). The BEL statistics appear to ignore the measurement errors and to ignore much of the time history information, so it would be somewhat surprising if it could do as well as the MACHO selection method.

Finally, Griest & Thomas (2004) have identified a serious logical flaw in the argument of Evans &

Belokurov (2004) who claim that the LMC microlensing optical depth must be lower than the MACHO value. The BEL analysis cannot seriously be considered as a method to select microlensing events from a complete data set of millions of light curves, because its false alarm rate is 1 in 10^4 , which is much higher than the microlensing rate for any plausible Galactic model. Thus, BEL use their method in the only way that they can, they apply it to events that have already passed the MACHO selection criteria. Thus, there is no chance that they could detect events that MACHO missed, so their detection efficiency is necessarily lower, contrary to the claim of Evans & Belokurov (2004). As we shall see in this paper, the BEL method fails to confirm 3 events that are almost certainly microlensing events, while “confirming” one microlensing candidate that is almost certainly a variable star. Thus, it seems clear that the current version of the BEL analysis does not help to identify actual microlensing events.

1.2. Paper Organization

This paper is organized as follows. Sec. 2 describes the data sets used for our analysis and the photometry codes used to convert the images into photometric measurements. Sec. 3 describes our method for light curve fitting and comparison with HST photometry of the candidate microlensed source stars. The detailed modeling of the 4 individual events presented in this paper are presented in sub-sections 3.1–3.4. A detailed comparison of the results of BEL’s analysis with our results and other additional data is presented in Sec. 4, and in Sec. 5, we discuss the implications of our results for the interpretation of the microlensing results towards the LMC.

2. Data and Photometry

2.1. MACHO Data

The events presented in this paper were all identified as microlensing candidates in Alcock et al. (2000c), based upon photometry with the standard MACHO SoDophot photometry routine. The SoDophot photometry presented in this paper is essentially identical to that presented in Alcock et al. (2000c). A subset of the MACHO images for these events were also reduced with the DifImPhot difference imaging photometry package (Tomaney & Crotts 1996). In very crowded star fields, the difference imaging method is usually more accurate than the profile fitting method employed by SoDophot (Alcock et al. 1999b, 2000b; Wozniak et al. 2001). Also, the SoDophot and DifImPhot photometry codes are likely to produce different systematic errors, so a comparison of SoDophot and DifImPhot photometry of the same images can reveal data points that might have be affected by these systematic errors.

2.2. Microlensing Alerts and CTIO Follow-up Data

Event MACHO-LMC-4 was the first LMC microlensing event discovered and announced in progress, and this occurred on 1994, Oct. 14. It was discovered while staffing arrangements for MACHO/GMAN service observing on the CTIO⁴ 0.9 m telescope were still being finalized, and as a consequence, it was not possible to take CTIO data through the peak of the event. Because of this problem with the CTIO data, extra observations were scheduled with the MACHO survey telescope (the 1.3m “Great Melbourne” telescope at Mt. Stromlo) until observations from CTIO could resume. The CTIO data set for this consists of a single observation before the light curve peak, taken shortly after the event was discovered, and 155 observations taken after the light curve peak, including 10 baseline observations taken more than a year after the peak. These CTIO data were reduced with the ALLFRAME package (Stetson 1994), and 0.5% was added in quadrature to the ALLFRAME error estimates to account for low level systematic errors such as flatfielding errors. (For the MACHO SoDophot photometry, 1.4% is added in quadrature to the SoDophot output errors as described in Alcock et al. (2000c).) 134 of these 156 measurements pass our data quality cuts (Alcock et al. 1996b) and are included in this analysis. This is in addition to 730 MACHO-red band and 728 MACHO-blue band photometric measurements from SoDophot which pass our data quality cuts, as well as 85 MACHO-red band and 78 MACHO-blue band images reduced with DifImPhot. The images reduced with DifImPhot were chosen to cover the region of the microlensing magnification as well as a bit of the baseline.

Microlensing event MACHO-LMC-13 was detected and announced on 1996, Feb. 11, near peak magnification as MACHO 96-LMC-1. Additional observations were immediately requested from the CTIO 0.9m, and 376 CTIO R-band images were eventually obtained including 145 baseline measurements taken more than 180 days after the light curve peak. 332 of these CTIO measurements pass our data quality cuts. The data from the MACHO survey includes 1074 MACHO-red measurements and 1176 MACHO-blue measurements reduced with SoDophot as well as 84 measurements covering the magnified part of the light curve in each MACHO band reduced with DifImPhot. In addition, there were 47 R-band and 64 V-band measurements from the UTSO 0.6m telescope. These are included in our fits, but they have only limited time coverage and have larger error bars than the CTIO measurements, and so they are not included in our figure. These data were reduced in the same way as the CTIO and LMC-4 data.

The final event in our sample is MACHO-LMC-15 which was detected and announced on 1997, Jan. 15 as MACHO 97-LMC-1, well before peak magnification. Additional observations were again immediately requested from the CTIO 0.9m, and 74 CTIO R-band images were obtained, including 26 baseline measurements taken more than 180 days after the light curve peak. 60 of these CTIO observations pass our data quality cuts. The MACHO survey data set consists of 475 MACHO-red and 586 MACHO-blue SoDophot measurements as well as 47 MACHO-red and 49 MACHO-blue DifImPhot measurements. The DifImphot data covers the magnified portion of the light curve along with the baseline immediately before and after the event.

⁴Cerro Tololo Inter-American Observatory, National Optical Astronomy Observatories, operated by the Association of Universities for Research in Astronomy, Inc., under cooperative agreement with the National Science Foundation.

Important constraints on our analysis of the light curve data come from the high resolution HST WFPC2 images of the microlensed source stars after the microlensing events were over. The reduction of the HST data and the identification of the microlensed source stars are discussed in (Alcock et al. 2001c; Nelson et al. 2005).

3. Testing the Microlensing Hypothesis with HST Constrained Light Curve Fitting

Unlike many types of stellar variability, it is possible to calculate theoretical microlensing light curves with an accuracy that is much better than observational errors, and this makes light curve fitting an extremely powerful method for testing the hypothesis that a candidate microlensing event was indeed caused by microlensing. The light curve fitting method is extremely effective in discriminating against the largest background to microlensing events in the LMC, supernovae of type Ia, as demonstrated in Alcock et al. (2000c). This success is due to the fact that there exist accurate models for type Ia supernova light curves. The situation is different for supernovae of type II, which do not have an accurate light curve model. The MACHO Project (Alcock et al. 2000c) was also able to exclude its type II SNe background by doing fits to SN type Ia light curve models, but this method was only convincing because these same events also had detectable galaxy hosts visible in the MACHO images or in other ground based images with slightly higher resolution. (Since type II SNe occur with young host stars and are usually fainter than type Ia SNe, they generally have much brighter host galaxies.)

After the removal of the supernovae, the confirmation of microlens candidates becomes a bit more difficult because little is known about the extremely rare types of variable stars that might mimic microlensing events. Thus, we are limited to testing the microlensing model rather than comparing it against another model. This task is complicated by the fact that the photometric errors are mildly non-Gaussian, although the MACHO and GMAN data have managed to remove most of the photometry outliers with cuts on a number of data quality flags. One model parameter that is particularly sensitive to systematic photometry errors is the baseline brightness of the source star. In the crowded fields observed by microlensing surveys, it is quite common for the source star to be blended with other stars within the same seeing disk. Thus, the source star brightness is usually used as a fit parameter, but there is a near degeneracy in light curve shapes that can make this parameter difficult to determine from a fit.

Another complication is the fact that $\sim 10\%$ of microlensing events are “exotic” events that don’t follow the standard Paczyński light curve. In some cases, such as caustic crossing binary lens events, the “exotic” features are so unique to lensing that there can be no ambiguity in the interpretation of the event, such as a caustic crossing binary lens event like MACHO-LMC-9 (Bennett et al. 1996). However, in other cases, such as MACHO-LMC-22 (Alcock et al. 2000c), non-microlensing variability can be fit with an exotic lens model.

In view of these considerations, we adopt the following series of steps in order to test the microlensing hypothesis for candidate microlensing events towards the LMC:

1. We fit each event with a light curve constraining the MACHO-blue source star brightness to match the V magnitude from the HST observations. (The transformation from MACHO-blue to the standard Cousins V-band is only weakly dependent on the MACHO-red magnitude (Alcock et al. 1999a).) The best unconstrained fit should not have a fit χ^2 that is significantly lower than the constrained fit—unless the source star itself is blended with the lens star.
2. The $\chi^2/\text{d.o.f.}$ values for the fit should be consistent with expectations for real microlensing event. Of particular interest are the $\chi^2/\text{d.o.f.}$ values for the follow-up CTIO and DifImPhot data points, and the $\chi^2/\text{d.o.f.}$ values in the light curve peak region (defined as the region where the best fit magnification is $A > 1.1$). Comparison of the different photometry data sets can indicate if an apparent deviation may be due to systematic photometry errors.
3. If a standard Paczyński model is not a good fit to the data, is there an exotic model that gives a good fit with plausible parameters? If so, are the number of candidates that must be fit with exotic models consistent with expectations?
4. The fit MACHO-red baseline magnitude for the source star is converted to the standard Cousins R-band and compared to the HST R-band magnitude of the source star. If it doesn't match, is it consistent with a blending model?

When making a goodness of fit judgement, it is important to keep in mind that the photometry errors are non-Gaussian, so Gaussian probabilities do not apply. Fig. 1 shows the distribution of fit $\chi^2/\text{d.o.f.}$ values for a set of Monte Carlo events from the LMC efficiency analysis (Alcock et al. 2001e) (black outline histogram) as well as the observed distribution for Galactic bulge microlensing events found by the MACHO alert system (Alcock et al. 1996b) (red histogram). Events that have been classified as “exotic” microlensing events can be expected to have a poor fit to a standard Paczyński light curve, and these are indicated by the red outline histogram. Note that all the events with $\chi^2/\text{d.o.f.} \geq 3$ have been displayed in the $\chi^2/\text{d.o.f.} = 3$ bin. The light curves for the events displayed in these histogram typically have 500–2000 total data points (including both MACHO-red and MACHO-blue observations), so the width of the $\chi^2/\text{d.o.f.}$ distribution is somewhat larger than we'd expect from Gaussian statistics. While there is considerable overlap between the Monte Carlo and actual Galactic bulge microlensing event fit $\chi^2/\text{d.o.f.}$ distributions, the real data distribution extends to larger values because some types of systematic photometry errors are not captured by the Monte Carlo simulations.

The fit $\chi^2/\text{d.o.f.}$ values for the events presented in this paper are listed in Table 1 and the fit $\chi^2/\text{d.o.f.}$ values for the events we present in this paper, LMC-4, 13, and 15, are in the 82nd, 64th, and 42nd percentiles, respectively, of the observed $\chi^2/\text{d.o.f.}$ distribution for non-exotic galactic bulge events (the solid red histogram in Fig. 1). In contrast, the dubious microlens candidate, LMC-23, is in the 91st percentile (see Sec. ??). This alone is not enough to disqualify this event as microlensing, particularly because a microlensing parallax model gives a significantly better $\chi^2/\text{d.o.f.}$.

Before proceeding to discuss the individual events, we should note that all the fits presented here are joint fits to the CTIO data as well as both the SoDophot and DifImPhot reductions of the MACHO data. This

is necessary because only the SoDophot reductions have been calibrated to the Cousins system and because the DifImphot photometry of the unmagnified portions of the light curves are limited. This means that the MACHO images that have yielded photometry by both methods are used twice, and we must be careful that this double counting does not affect our results. In order to correct for the effects of this double counting, we have adjusted the error bars in Table 1 to coincide with the fractional errors obtained by fitting only the SoDophot+CTIO data or the DifImPhot+CTIO data (whichever has smaller error estimates). Also, the total $\Delta\chi^2$ values presented in Table 3 are the sum of the individual $\Delta\chi^2$ values for the CTIO data plus the larger of the SoDophot or the DifImphot $\Delta\chi^2$ values.

3.1. Event MACHO LMC-4

The full MACHO LMC-4 light curve is shown in Fig. 2 and Fig. 3 shows a light curve close-up. The black curve in each plot is the best fit standard Paczyński light curve, while the fit parameters and χ^2 values are given in Tables 1 and 2. The fit χ^2 decreases by only 0.16 with one additional degree of freedom, if the HST constraint on the baseline brightness in the MACHO-blue band is released. The data in Fig. 2 have been combined into 8-day bins and the data shown in Fig. 3 are displayed in 2-day bins in order to show how well the data fits the model light curve. Since there are as many as 5 observations per day for this event, a display without binning is easily dominated by the measurements with large error bars, and the strength of the signal is easily obscured (as shown in (Belokurov, Evans & Le Du 2004)). The DifImPhot photometry provides error bars that are $\sim 75\%$ of the SoDophot error bars, and the fit $\chi^2/\text{d.o.f.}$ values are similar. The CTIO photometry has error bars that average $\sim 42\%$ of the SoDophot error bars with $\chi^2/\text{d.o.f.} \simeq 1$, so the DifImPhot and CTIO photometry clearly support the microlensing model.

Table 3 shows $\Delta\chi^2$, which is the improvement in the fit χ^2 over a constant brightness model. As we should expect from the size of the error bars, the $\Delta\chi^2$ values are about a factor of two larger for the DifImPhot data than with the original SoDophot data. The $\Delta\chi^2$ contribution from the CTIO data is smaller, despite the smaller error bars, because of limited coverage of the CTIO observations.

The one apparent discrepancy between the model and the data is the MACHO-blue point at the peak of the light curve, a bin which is the average of the 6 observations from the night of 1994, Oct. 20, and 2 observations from Oct. 21, when most of the night was clouded out. This high point is caused by 3 of these 8 unbinned measurements, which are between $2\text{-}\sigma$ and $3\text{-}\sigma$ above the best fit curve with the SoDophot photometry. 4 of the remaining measurements from these two days are within $1 - \sigma$ of the best fit curve, and the remaining point is about $1.8\text{-}\sigma$ below the best fit curve. The 3 high points are immediately preceded and followed by other observations on the same day that are within $1\text{-}\sigma$ of or below the best fit light curve. For the DifImPhot photometry, the 3 high points are between $1.5\text{-}\sigma$ and $2.2\text{-}\sigma$ above the best fit curve, but the point below the curve has moved much closer to the fit curve. So, although the DifImPhot photometry reduces the scatter, the average of the 8 data points is $\sim 3\text{-}\sigma$ above the curve for both the SoDophot and DifImPhot photometry.

All evidence suggests that these high photometry points are due to a systematic photometry errors

instead of some intrinsic change in blue-band brightness variation. The high points are not correlated in time, and they are not reproduced in the MACHO-red band despite the fact that the two MACHO passbands have some overlap in wavelength. This strongly suggests that this high point is due to a systematic photometry error, and observers report suggests a possible cause of such an error. The report from Oct. 20 began with the following description of the observing conditions: ‘Observing conditions fairly poor for most of the night, drifting cloud patches and a bright moon. Seeing poor, 2.7”–3.5”.’ These bright moon conditions did not affect any other part of the magnified part of the light curve, so we conclude that a systematic photometry error related to the bright sky background is the most likely cause of the MACHO-blue deviation at the peak of the light curve.

The source star lies on the main sequence in the HST color-magnitude diagram (Alcock et al. 2001c; Nelson et al. 2005), and its fit R-magnitude is within $1-\sigma$ of the HST R-magnitude, so the microlensing model correctly predicts the source star color. (The uncertainty in the fit R_M magnitude is the quadrature sum of the fit error (0.04 mag in this case), the 0.04 mag calibration uncertainty (Alcock et al. 1999a), and the uncertainty in the HST V-magnitude that the fit is normalized to (0.03 mag). Table 3 shows $\Delta\chi^2$, the improvement in χ^2 between the microlens model fit and a constant brightness star fit. While the CTIO data provide substantially more precise photometry than the Mt. Stromlo data, the much better light curve coverage means that most of strength of the microlensing signal comes from the Mt. Stromlo data. The addition of the CTIO data and the DifImphot photometry strengthens the microlensing signal considerably, from $\Delta\chi^2 = 11,518$ (from the SoDophot photometry alone) to $\Delta\chi^2 = 27,973$ (from the DifImphot photometry and CTIO data), with no indication of a deviation from the Paczyński light curve (aside from the apparent systematic error at the light curve peak). The $\Delta\chi^2$ value for LMC-4 with the CTIO and DifImPhot photometry ranks it second among on the MACHO LMC microlensing event candidates, behind LMC-14 (Alcock et al. 2001b) and in an approximate tie with LMC-1.

3.2. Event MACHO LMC-13

Figs. 4 and 5 show the full light curve and a close-up of the LMC-13 light curve, which is displayed in 8 and 4-day bins, respectively. This event shows the greatest improvement with the DifImphot photometry, with DifImPhot error bars that are, on average, $\sim 67\%$ of the SoDophot error bars. Also, in this case, CTIO observations were able to begin shortly after the alert, just prior to peak magnification, and the CTIO data show that the light curve follows the microlensing model very accurately from peak magnification down to to the baseline. Fig. 5 also reveals some apparent photometric errors in the SoDophot MACHO-blue light curve. Apparent deviations above the fit curve at the peak and near day 1575 disappear in the DifImPhot data set as does a low point with small error bars near day 1485. These systematic errors also appear to interfere with the blending estimate from the light curve fit. An unconstrained fit predicts a source star V magnitude that misses the HST value by about 3.4 times the $1-\sigma$ uncertainty, and the fit with the source star magnitude constrained to the HST magnitude increases the χ^2 value of the fit by 7.08 which corresponds to a $2.7-\sigma$ discrepancy. However, most of this χ^2 is from the MACHO-blue SoDophot photometry while the MACHO-blue DifImphot photometry has an improved χ^2 with the HST normalized fit. Thus, we believe

that the HST normalized fit is probably more accurate.

From Table 1, we can see that our fit matches the HST R-magnitude exactly, and the source star is on the main sequence of the HST color-magnitude diagram (Nelson et al. 2005). While the DifImPhot photometry reduces the photometry error bars by a factor of 2/3, the CTIO follow-up photometry has error bars that are, on average a factor of 5 smaller than the original SoDophot photometry of the MACHO data. The fact that the Paczyński light curve shape is confirmed with photometry 5 times more accurate than the MACHO SoDophot photometry that the event identification was based on provides strong support for the microlensing interpretation of this event.

3.3. Event MACHO LMC-15

The full light curve of MACHO LMC-15 is shown in Fig. 6 in 8-day bins, a close-up is shown in Fig. 7, displayed in 2-day bins. This event was the lowest signal-to-noise event to pass the stricter “criterion A” of the MACHO LMC 5.7 year analysis. Fortunately, the event was identified well before peak magnification, and very good light curve coverage was obtained from CTIO that filled the gaps in the data from Mt. Stromlo. Furthermore, the error bars on the CTIO measurements are, on average, a factor of 4 smaller than the MACHO-red error bars and a factor of 4.8 smaller than the MACHO-blue error bars, while the CTIO $\chi^2/\text{d.o.f.}$ is quite reasonable. So, the CTIO data provides strong confirmation of the microlensing hypothesis. The DifImPhot photometry, on the other hand, provides only a modest improvement over SoDophot with error bars that are $\sim 85\%$ of the SoDophot error bars in the MACHO-red band and $\sim 95\%$ of the SoDophot error bars in the MACHO-blue band.

The fit parameters presented Table 1 indicate that the fit R-band magnitude matches the HST value to better than 0.5σ , and the source star is also on the HST main sequence (Nelson et al. 2005). Also, the constraint that the MACHO-blue magnitude be fixed to match the HST V-band magnitude only causes χ^2 to increase by 0.39, so the fit V-band magnitude also matches the HST V-band magnitude to better than $1-\sigma$.

3.4. Counterexample: Event MACHO LMC-23

Microlensing event candidate MACHO LMC-23 was not detected by the MACHO alert system, so there is no CTIO data for it. Some DifImphot photometry does exist, with error bars that average $\sim 60\%$ of the SoDophot error bars. It is obvious from Fig. 8 that there are deviations from the standard Paczyński light curve fit. Both the MACHO-red and blue data are brighter than the standard Paczyński light curve fit near days 1123 and 1163, and this occurs for both the SoDophot and DifImPhot photometry. All 4 data sets appear to be below the fit curve near day 1180, as well. A microlensing parallax model (the dashed green line) provides a much better fit, and seems to fit the deviations at days 1163 and 1180. There still appears to be a deviation near day 1123, however.

These qualitative observations are also reflected in the fit χ^2 values shown in Table 2. For the standard

Paczynski light curve fit, the peak $\chi^2/\text{d.o.f.}$ values are quite large ranging from 3.229 for the MACHO-blue SoDophot data to 5.814 for the blue DifImPhot data. For the microlensing parallax model fit (labeled *LMC-23-p*), the $\chi^2/\text{d.o.f.}$ values drop to reasonable values for the SoDophot photometry (except perhaps the peak $\chi^2/\text{d.o.f.}$ value for the MACHO-red data), but the DifImPhot values remain high at 2.434 and 3.012, respectively, for MACHO-red and blue. This suggests that neither model is likely to be correct, but it is possible that a binary lens model might do better.

Another problem is that the fit R-band magnitudes do not match the HST R-band magnitude. They are off by $V - R \approx 0.3$, which is more than $4\text{-}\sigma$ for both the standard and parallax fit. The source star is on the sub-giant branch of the HST color magnitude diagram (Nelson et al. 2005), but the color at maximum brightness is more consistent with a main sequence star. On the other hand, the apparent redness of the source star could possibly be explained by blending in the HST images if the lens star were visible and redder than the source, as was the case for event 5 (Alcock et al. 2001d).

However, an additional complication is the fact that the EROS Collaboration has observed a subsequent brightening of this star approximately 2500 days after the one observed by MACHO (Glicenstein 2004). Multiple brightening episodes can occur in binary lens or binary source microlensing events, such as MACHO 96-BLG-4 (Alcock et al. 2000a), if the binary lens or source separation is large. However, the probability of detecting such an event decreases in proportion to the binary separation because alignment of both members of the binary with the single lens or source decreases with their separation. Thus, while it might be possible to find a model that could explain this event as lensing, it would require several highly improbable occurrences for this single event: two different types of exotic lensing to explain the light curve shape in the MACHO data as well as the brightening seen by EROS, plus a bright lens (or unlikely HST blend by chance superposition). It is much more likely that MACHO LMC-23 is a variable star. This is currently the only MACHO LMC microlens candidate that we have any reason to suspect is not an actual microlensing event.

4. Confrontation of BEL Event Classification with Additional Data

The classification of the MACHO LMC events by the MACHO team and BEL are listed in Table 4. This table also provides a “confirmation” column which indicates the implication of additional data for the event classification. Items that support the microlensing interpretation are listed in bold face, and items that tend to contradict the microlensing interpretation are presented in italics. The MACHO verdict refers to the classification given in A00. Events listed as $\mu\text{lens-A}$ and $\mu\text{lens-B}$ are candidate microlensing events that passed the strict criteria A, or only the looser B criterion. Event 22 did pass criteria B, but a spectrum taken with the MSSSO 2.3m telescope revealed that the source was an emission line galaxy at $z = 0.233$ (T. Axelrod, private communication).

Table 4 indicates that our expectation that the BEL event selection method is unreliable has been borne out by our new data and analysis. Of the 4 events that we have analyzed, the only one that BEL classify as microlensing is event 23, which is most likely a variable star. The other 3 events they classify as non-

microlensing, but the new data confirms the microlensing interpretation, again contradicting BEL. These 4 events probably provide the best test of the BEL method, because these data had not been previously published, except in a PhD thesis (Becker 2000), and so, the additional data were probably not seen by BEL when they were designing their method. In contrast, the original MACHO analysis (Alcock et al. 2000c) is confirmed for the three events with additional photometric data during the microlensing event, but not for event 23.

The complete MACHO analysis identifies 25 events as either microlensing candidates or supernovae. (The events are numbered 1, 4–27, as events 2 and 3 from the first year analysis (Alcock et al. 1996a) do not make the 5–year cuts.) Of these 25 events, MACHO classifies 16 as microlensing candidates, 8 as background supernovae, and 1 as either an AGN or a peculiar background supernova. The BEL analysis identifies 10 of these events as microlensing, 5 as supernovae, and 9 as neither. Event 9, the LMC binary lens event (Bennett et al. 1996; Alcock et al. 2000a), is not considered by BEL. The BEL analysis agrees with MACHO in the classification of 7 events as microlensing and 4 events as supernovae. We will now examine these classifications in light of other, non–light curve data.

Of the 7 events identified by both MACHO and BEL as microlensing, event 1 has a follow-up spectrum consistent with the microlensing interpretation (della Valle 1994), and event 5 has been confirmed by HST observations that identified the lens star in the Milky Way disk and provided the first complete solution for a microlensing event (Alcock et al. 2001d; Drake, Cook, & Keller 2004; Gould, Bennett, & Alves 2004; Nguyen et al. 2004). Event 14 was confirmed with high signal-to-noise GMAN follow-up data which also enabled measurement of the microlensing “xallarap” effect (light curve oscillations due to the orbit of a binary source star) and the determination that the lens is close to the LMC (Alcock et al. 2001b). We argue in Sec. 5 that events 1 and 25 are very likely to be microlensing, as well, but we have seen that event 23 is probably a variable star although it was identified as a microlensing candidate by both MACHO (Alcock et al. 2000c) and BEL. Thus, 4 of these 7 events can be considered to be confirmed, and 1 is rejected.

Three events are identified by BEL, but not MACHO, as microlensing: events 10, 22, and 24. They all have highly asymmetric light curves that suggest a non-microlensing origin, although in the case of event 22, the asymmetry can be fit by a microlensing parallax model with plausible parameters. The MACHO photometry of event 10 is a near perfect fit to a supernova type Ia light curve, and so this event is clearly a background supernova. It is near the blue end of the SN type Ia color distribution, and this is probably why BEL’s SN test fails. Event 24 is also fit much better by a supernova type Ia light curve than by standard microlensing, so it was also rejected as a microlensing candidate. The quality of the type Ia fit for event 24 is poor, however, so it is more likely that this event is a type II supernova. The source locations for each of these events correspond to background galaxies. For event 24, the galaxy is visible in the MACHO images, while the source “star” for event 10 is revealed to be a compact galaxy in HST images (Alcock et al. 2001c). The source for LMC-22 appears slightly extended in a higher resolution CTIO 4m frame, and a spectrum of the source indicates that it is probably an active galaxy. Thus, the microlensing interpretation is rejected for all three of these events classified by BEL, but not MACHO, as microlensing.

Of the 9 events classified by BEL as neither microlensing nor supernovae, MACHO classifies 2 as

supernovae, and 7 as microlensing (events 4, 7, 8, 13, 15, and 18). In Secs. 3.1–3.3, we have shown that the microlensing interpretations of 3 of these events (4, 13, and 15) are strongly confirmed by the additional photometry we have presented, but there exists no follow-up data that sheds light on the other events. However, event 8 is the lone event in the center of the LMC bar, where the LMC self-lensing probability is highest (Mancini, Calchi Novati, Jetzer, & Scarpetta 2004), so it seems likely that this event is microlensing, as well. Thus, the BEL classification fails for 3 of these events and is likely to fail for one other.

It seems clear that the only category in which BEL’s event classification scheme appears to succeed, more often than not, is when it agrees with the MACHO classification. We have shown that their identification of events as “non-microlensing” fails for the 3 events with new data presented in this paper, and in most cases where they disagree with MACHO, additional data strongly suggests that BEL is wrong. We can only conclude that BEL’s selection method does not provide any help in separating real microlensing events from other types of variability that mimic microlensing. However, this does not mean that neural networks cannot improve upon the MACHO analysis. Instead, as we have argued in Sec. 1.1, that BEL’s method fails because of the weak set of statistics that they have relied upon. A neural network that uses the more powerful light curve fitting based statistics used by MACHO might indeed offer an improvement.

5. Discussion and Conclusions

The MACHO Project’s 5.7 year LMC analysis has identified a set of 16 candidate LMC microlensing events after removing the background supernovae. In this paper, we have analyzed additional photometry from GMAN follow-up observations with the CTIO 0.9m telescope as well as DifImPhot photometry of the original Mt. Stromlo MACHO observations for three of these events: MACHO LMC-4, 13 and 15. This additional photometry has errors that are smaller than the original MACHO photometry by a factor of 1.1-1.5 (for DifImPhot) and of 2.4-5 (for the GMAN CTIO photometry), and improves the light curve time coverage for these events. All three light curves with the improved photometry are well fit by a standard Paczyński microlensing model.

For two of the three light curves, the fit accurately predicts both the V and R-band magnitudes from high resolution HST observations of the microlensed source star. For the other event, LMC-13, the unconstrained Paczyński fit predicts a V-band magnitude that differs by the HST magnitude by $2.7\text{-}\sigma$, but the difference between the DifImPhot and SoDophot photometry of the Mt. Stromlo data suggests that this may be affected by low level systematic photometry errors. A Paczyński light curve fit constrained to the HST V magnitude accurately predicts the HST R magnitude for event LMC-13. Thus, it is fair to say that the additional photometry provides a strong confirmation of the microlensing interpretation of these three events.

In addition to these events, there are several other of the MACHO LMC microlensing candidates for which the microlensing interpretation seems very secure. Event 14 has also been confirmed with GMAN photometry that provides evidence of the “xallarap” effect (Alcock et al. 2001b), and Event 5 is the first

microlensing event in which the lens has been detected (Alcock et al. 2001d; Drake, Cook, & Keller 2004; Nguyen et al. 2004) and has been completely solved yielding the mass, transverse velocity and distance of the lens (Gould, Bennett, & Alves 2004). The consistency of the microlensing mass determination with the lens star brightness and colors provides a strong confirmation of the microlensing model for this event.

Events LMC-1 and LMC-25 are the two events which clearly have red clump giant source stars (della Valle 1994; Alcock et al. 2000c; Nelson et al. 2005), and such stars have not exhibited the type of variability that could be confused with microlensing (Keller et al. 2002) as observed in EROS LMC-1 and 2 and MACHO LMC-2 and 23 (Alcock et al. 1997b; Ansari et al. 1995; Beaulieu et al. 1995; Lasserre et al. 2000; Glicenstein 2004). Finally, event MACHO LMC-9 is well fit by a binary lens model (Bennett et al. 1996; Alcock et al. 2000a) and has a light curve shape that is different from other known forms of variability with the very rapid brightness variation that is characteristic of a binary lens caustic crossing.

So, out of the 16 MACHO LMC microlensing candidates, 5 have been confirmed with additional data, and another 3 appear very likely to be microlensing. Of the 5 events that have been confirmed with additional data, 4 have been selected by a completely independent method—their discovery by the MACHO alert system. All 4 of these events have been confirmed to be microlensing, which suggests that most of the MACHO LMC microlensing candidates are indeed due to microlensing. Nevertheless, the example of MACHO LMC-23 suggests that some caution is warranted regarding the interpretation of 7 remaining MACHO LMC microlensing events that have not yet been confirmed.

It is instructive to consider the results of Mancini, Calchi Novati, Jetzer, & Scarpetta (2004) who have done detailed predictions of the properties of LMC self-lensing events based upon some of the latest models of the LMC. (Their classifications are listed in Table 4.) They identify 4 of the MACHO events that are good LMC self-lensing candidates: events 6, 8, 13, and 14. A straight-forward extension of their analysis also adds the binary lens event, 9, to this list. This identification is strengthened by independent light curve analyses that suggest that events 9 and 14 both have lenses residing in the LMC (Bennett et al. 1996; Alcock et al. 2001b). Of the remaining 10 events, the event 5 lens star has been shown to be a disk star. It is most likely a member of the thick disk, but thin disk membership cannot be ruled out (Gould, Bennett, & Alves 2004). Event 20 is also a disk lens candidate because it appears to be blended with a star that is much redder than other LMC stars of similar magnitude (Alcock et al. 2000c). (If event 20 is also a disk lens this would give us a total of 2 disk events when a total of 0.75 are expected from the combined thin and thick disks. The Poisson probability to detect 2 or more disk events when 0.75 are expected is 17%.) This leaves 8 events as halo lens candidates: events 1, 4, 7, 15, 18, 21, 25 and 27. Two of these halo lens candidates (4 and 15) are confirmed by the photometry and light curve fitting presented here, and two others (1 and 25) are considered “solid” events because of their red clump giant source stars. Thus, there is little difference between the quality of the different categories of events. Thus, the “confirmed” events appear to be distributed about evenly among the disk, halo, and LMC-self lensing candidate events.

Our qualitative conclusion is that the puzzle of the excess LMC lensing events remains unresolved. Our knowledge of the Galactic disk and LMC suggest that most of the lenses must reside in a previously undiscovered population, and the Milky Way halo is the natural location for this, since the halo’s mass is

largely unaccounted for. But such a population presents a number of problems if it is composed of known objects like white dwarfs. The leading alternative explanation is that LMC self-lensing dominates, but this possibility gets no significant observational support from detailed LMC models or from the properties of the microlensing events themselves. (See Sahu (2003) for a different point of view.)

A resolution of this puzzle will probably require additional data so that the distance to a representative sample of LMC lensing events can be determined. This could come from the microlensing key project for the SIM mission (Unwin & Turyshev 2002), or from a Deep Impact mission extension (DIME) (Cook et al. 2003), which would use the 30cm telescope on the Deep Impact spacecraft to make microlensing parallax observations from a Heliocentric orbit (Gould 1995a), if it is approved. Microlensing experiments towards other lines of site could also shed some light on this issue (deJong et al. 2004; Calchi Novati et al. 2005; Paulin-Henriksson et al. 2003). In addition, the SuperMACHO (Becker 2004) and MOA-II (Muraki 2004) surveys expect to substantially increase the detection rate of LMC microlensing events in order to provide alerts for SIM and DIME and to measure the spatial variation of the microlensing optical depth across the face of the LMC.

D. P. B. was supported by grants AST 02-06189 from the NSF and NAG5-13042 from NASA.

REFERENCES

- Afonso, C., et al. 2000, *ApJ*, 532, 340
- Afonso, C., et al. 2003, *A&A*, 400, 951
- Afonso, C., et al. 2003, *A&A*, 404, 145
- Albrow, M. D., et al. 1999, *ApJ*, 522, 1011
- Albrow, M. D., et al. 2001, *ApJ*, 556, L113
- Alcock, C., et al. 1993, *Nature*, 365, 621
- Alcock, C., et al. 1996a, *ApJ*, 461, 84
- Alcock, C., et al. 1996b, *ApJ*, 463, L67
- Alcock, C., et al. 1997a, *ApJ*, 479, 119; (E) 500, 522
- Alcock, C., et al. 1997b, *ApJ*, 486, 697
- Alcock, C. et al. 1998, *ApJ*, 499, L9
- Alcock, C., et al. 1999a, *PASP*, 111, 1539
- Alcock, C., et al. 1999b, *ApJ*, 521, 602

- Alcock, C., et al. 2000a, *ApJ*, 541, 270
- Alcock, C., et al. 2000b, *ApJ*, 541, 734; (E) 557, 1035
- Alcock, C. et al. 2000c, *ApJ*, 542, 281
- Alcock, C., et al. 2001a, *ApJ*, 550, L169
- Alcock, C., et al. 2001b, *ApJ*, 552, 259
- Alcock, C., et al. 2001c, *ApJ*, 552, 582
- Alcock, C., et al. 2001d, *Nature*, 414, 617
- Alcock, C., et al. 2001e, *ApJS*, 136, 439
- Alves, D. R. 2004, *ApJ*, 601, L151
- Ansari, R., et al. 1995, *A&A*, 299, L21
- Aubourg, E. et al. 1993, *Nature*, 365, 623
- Beaulieu, J. P., et al. 1995, *A&A*, 299, 168
- Becker, A. C. 2000, PhD thesis, University of Washington
- Becker, A. C. 2004, ArXiv Astrophysics e-prints, astro-ph/0409167
- Belokurov, V., Evans, N.W. & Le Du, Y. 2003, *A&A*, 341, 1373
- Belokurov, V., Evans, N.W. & Le Du, Y. 2004, *A&A*, 352, 233
- Bennett, D. P., et al. 1996, *Nucl. Phys. B (Proc. Suppl.)*, Vol. 51B, 131
- Bennett, D. P., & Rhie, S. H., 1996, *ApJ*, 472, 660
- Bond, I. A., et al. 2004, *ApJ*, 606,
- Brook, C. B., Kawata, D., & Gibson, B. K. 2003, *MNRAS*, 343, 913
- Calchi Novati, S., et al. 2005, ArXiv Astrophysics e-prints, astro-ph/0504188
- Cook, K., et al., 2003, *BAAS*, 20314302
- deJong, J.T.A. et al., 2004, *A&A*, 417, 461
- della Valle, M. 1994, *A&A*, 287, L31
- Drake, A. J., Cook, K. H., & Keller, S. C. 2004, *ApJ*, 607, L29
- Evans, N. W., & Belokurov, V. 2004, ArXiv Astrophysics e-prints, astro-ph/0411222

- Evans, N. W., & Kerins, E. 2000, *ApJ*, 529, 917
- Flynn, C., Holopainen, J., & Holmberg, J. 2003, *MNRAS*, 339, 817
- García-Berro, E., Torres, S., Isern, J., & Burkert, A. 2004, *A&A*, 418, 53
- Gates, E. I. & Gyuk, G. 2001, *ApJ*, 547, 786
- Glicenstein, J.-F. 2004, talk presented at the Hawaii Microlensing Workshop 2004,
<http://www.stelab.nagoya-u.ac.jp/hawaii/>
- Gould, A. 1995a, *ApJ*, 441, L21
- Gould, A. 1995b, *ApJ*, 441, 77
- Gould, A., Bennett, D. P., & Alves, D. R. 2004, *ApJ*, 614, 404
- Griest, K., & Thomas, C. L. 2005, *MNRAS*, 359, 464
- Gyuk, G., Dalal, N., & Griest, K. 2000, *ApJ*, 535, 90
- Han, C. & Gould, A. 1996, *ApJ*, 467, 540
- Holopainen, J. & Flynn, C. 2004, *MNRAS*, 351, 721
- Jetzer, P., Mancini, L., & Scarpetta, G. 2002, *A&A*, 393, 129
- Keller, S. C., Bessell, M. S., Cook, K. H., Geha, M., & Syphers, D. 2002, *AJ*, 124, 2039
- Lasserre, T., et al. 2000, *A&A*, 355, L39
- Lennon, D. J., Mao, S., Fuhrmann, K., & Gehren, T. 1996, *ApJ*, 471, L23
- Mancini, L., Calchi Novati, S., Jetzer, P., & Scarpetta, G. 2004, *A&A*, 427, 61
- Mao, S. & Paczyński, B. 1991, *ApJ*, 374, L37
- Minniti, D., Vandehei, T., Cook, K. H., Griest, K., & Alcock, C. 1998, *ApJ*, 499, L175
- Muraki, Y. 2004, talk presented at the Hawaii Microlensing Workshop 2004,
<http://www.stelab.nagoya-u.ac.jp/hawaii/>
- Nelson, C., et al. 2005, *AJ*, submitted.
- Nguyen, H. T., Kallivayalil, N., Werner, M. W., Alcock, C., Patten, B. M., & Stern, D. 2004, *ApJS*, 154, 266
- Nikolaev, S., Drake, A. J., Keller, S. C., Cook, K. H., Dalal, N., Griest, K., Welch, D. L., & Kanbur, S. M.
2004, *ApJ*, 601, 260
- Paczynski, B. 1986, *ApJ*, 304, 1

- Paulin-Henriksson, S., et al., 2003, *A&A*, 405, 15
- Popowski, P., et al. 2004, *ArXiv Astrophysics e-prints*, astro-ph/0410319
- Rahvar, S. 2004, *MNRAS*, 347, 213
- Rahvar, S. 2005, *MNRAS*, 356, 1127
- Refsdal, S. 1966, *MNRAS*, 134, 315
- Rhie, S. H. et al. 2000, *ApJ*, 533, 378
- Sahu, K. C. 1994, *Nature*, 370, 275
- Sahu, K. C. 2003, *The Dark Universe: Matter, Energy and Gravity*, 14
- Salim, S., Rich, R. M., Hansen, B. M., Koopmans, L. V. E., Oppenheimer, B. R., & Blandford, R. D. 2004, *ApJ*, 601, 1075
- Schechter, P. L., Mateo, M., & Saha, A. 1993, *PASP*, 105, 1342
- Spagna, A., Carollo, D., Lattanzi, M. G., & Bucciarelli, B. 2004, *A&A*, 428, 451
- Stetson, P. B. 1994, *PASP*, 106, 250
- Sumi, T. et al. 2003, *ApJ*, 591, 204
- Tomaney, A. B. & Crotts, A. P. S. 1996, *AJ*, 112, 2872
- Torres, S., García-Berro, E., Burkert, A., & Isern, J. 2002, *MNRAS*, 336, 971
- Udalski, A., Szymański, M., Kałużny, J., Kubiak, M., Krzmiński, W., Mateo, M., Preston, G. W., & Paczyński, B. 1993, *Acta Astronomica*, 43, 289
- Udalski, A. et al. 1994a, *Acta Astronomica*, 44, 165
- Udalski, A., Szymański, M., Kałużny, J., Kubiak, M., Mateo, M., Krzmiński, W., & Paczyński, B. 1994b, *Acta Astronomica*, 44, 227
- Uglesich, R. R., Crotts, A. P. S., Baltz, E. A., de Jong, J., Boyle, R. P., & Corbally, C. J. 2004, *ApJ*, 612, 877
- Unwin, S. & Turyshev, S., 2002,
planetquest.jpl.nasa.gov/Navigator/library/science_AAS_Jan02.pdf
- von Hippel, T., Sarajedini, A., & Ruiz, M. T. 2003, *ApJ*, 595, 794
- Weinberg, M. D. 2000, *ApJ*, 532, 922
- Wozniak, P. R., Udalski, A., Szymanski, M., Kubiak, M., Pietrzynski, G., Soszynski, I., & Zebrun, K. 2001, *Acta Astronomica*, 51, 175.

Wu, X. 1994, *ApJ*, 435, 66

Zhao, H., Ibata, R. A., Lewis, G. F., & Irwin, M. J. 2003, *MNRAS*, 339, 701

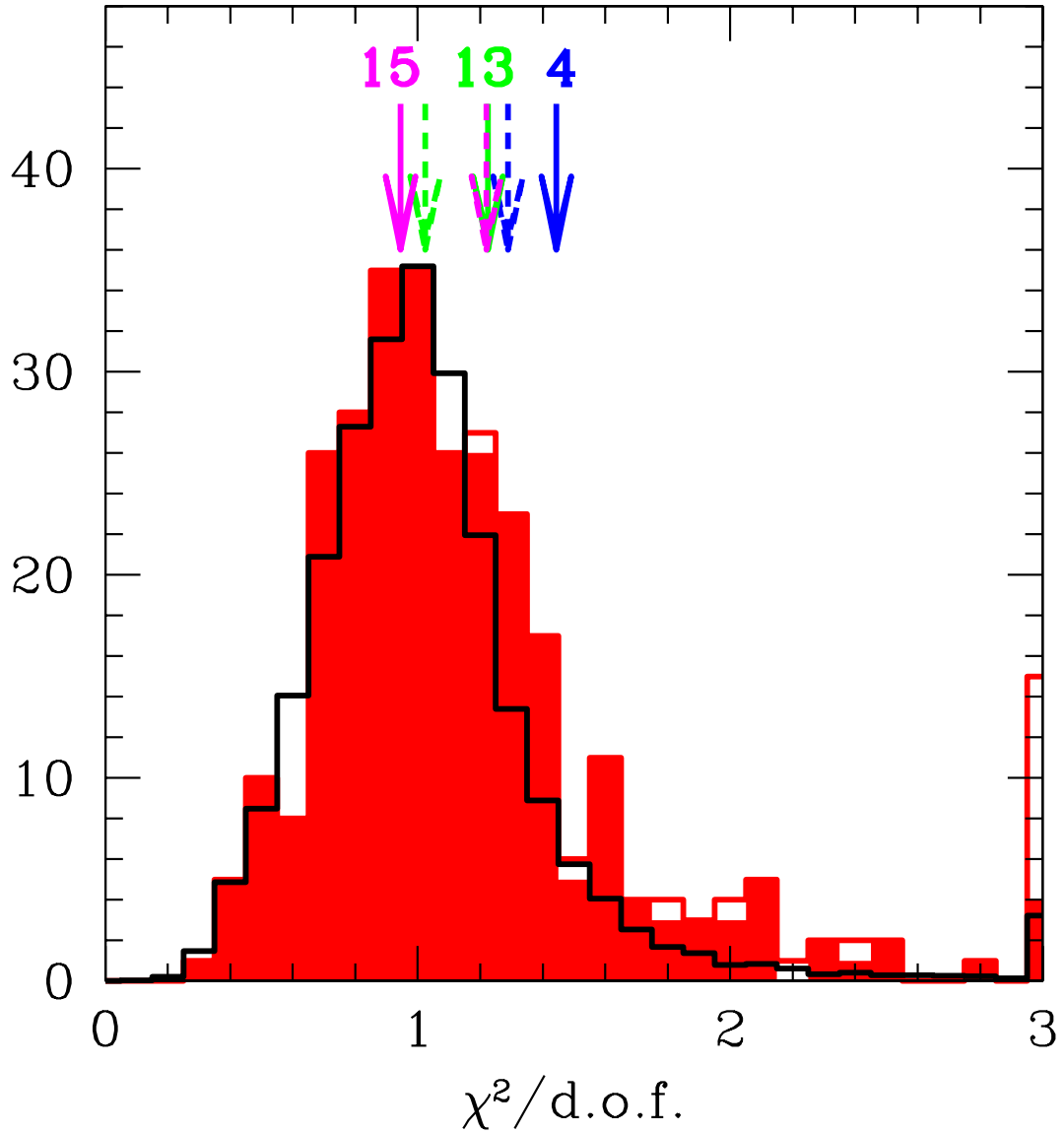


Fig. 1.— The distribution of reduced $\chi^2/\text{d.o.f.}$ for microlensing light curve fits is shown for simulated events in the MACHO LMC data (black histogram) and for observed Galactic bulge events (solid red histogram). The unfilled part of the red histogram indicates non-standard microlensing events, such as microlensing parallax and binary lens events. The solid arrows indicate the fit $\chi^2/\text{d.o.f.}$ values for the MACHO observations of three events presented here: MACHO-LMC-4, 13 and 15. The dashed arrows indicate the $\chi^2/\text{d.o.f.}$ values for the additional photometry presented in this paper.

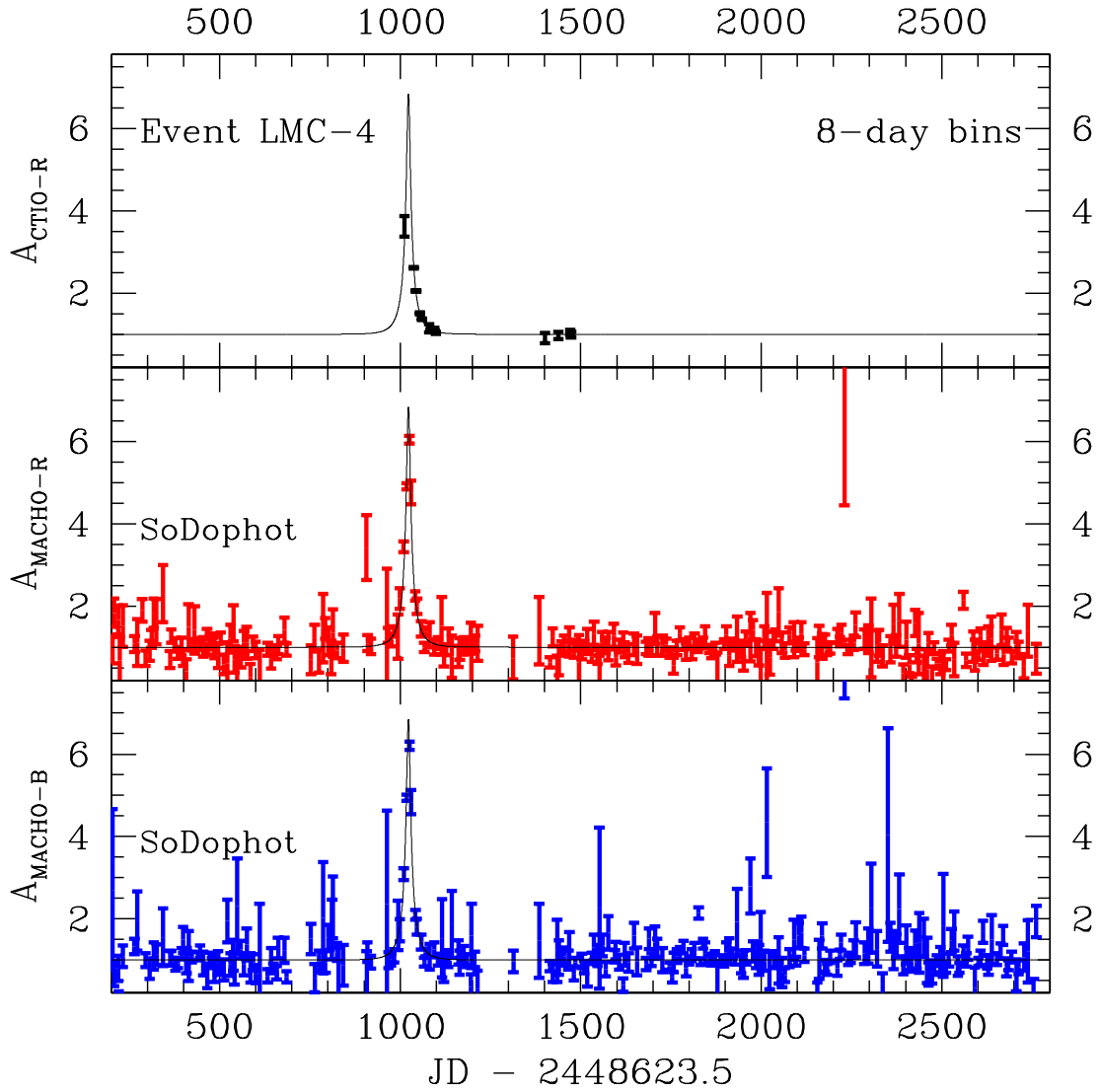


Fig. 2.— The MACHO and GMAN-CTIO (top panel) follow-up data are shown in the full light curve for microlensing event LMC-4. The solid line is the best fit light curve constrained to match the HST V-band magnitude, and all data is presented in 8-day bins.

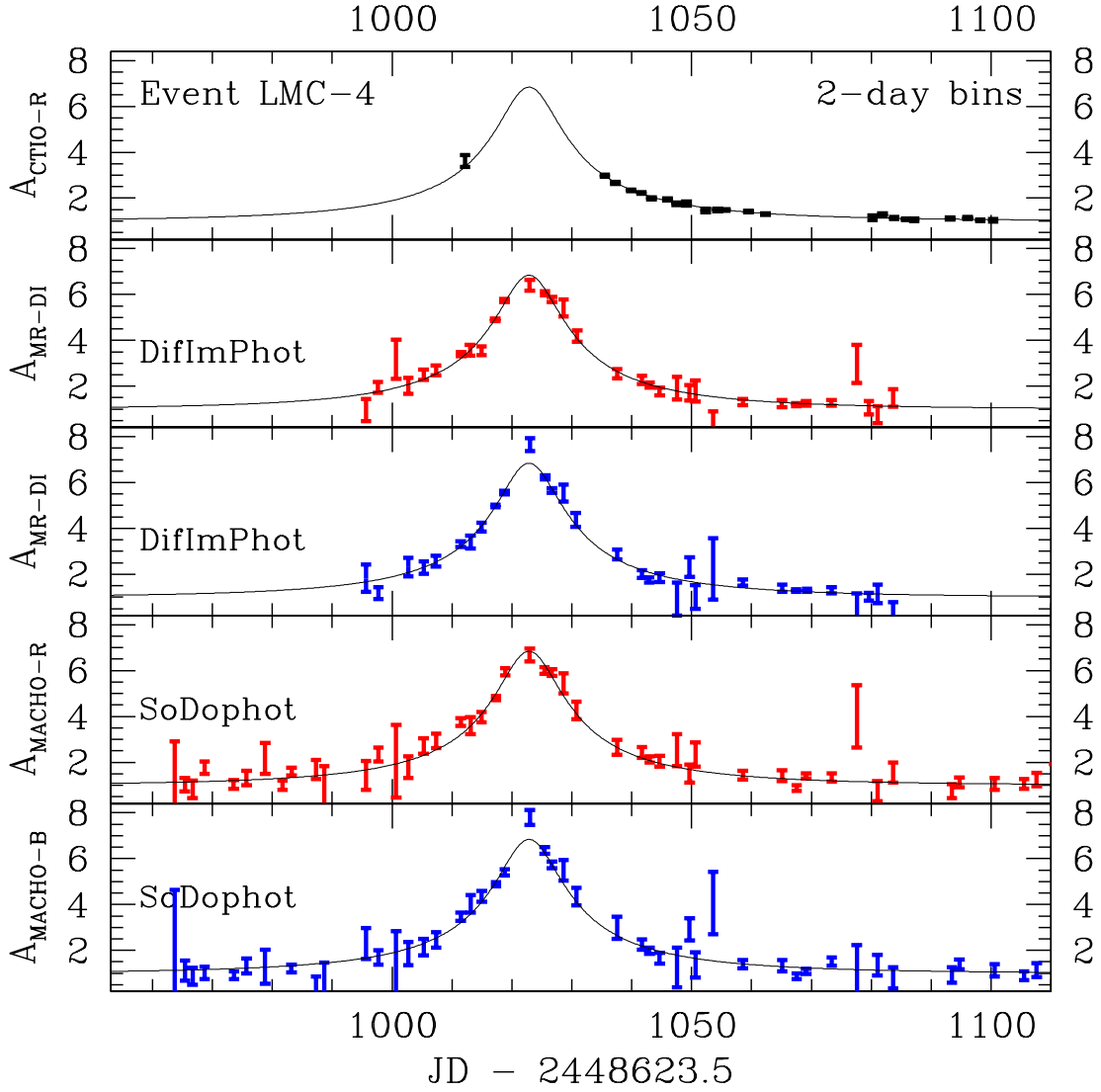


Fig. 3.— The MACHO and GMAN-CTIO (top panel) follow-up data are shown in a close-up of the light curve for microlensing event LMC-4. All data is presented in 2-day bins, and the 2-band MACHO data is presented with the original SoDophot photometry (bottom 2 panels) as well as photometry from the DifImPhot package (2nd and 3rd panels).

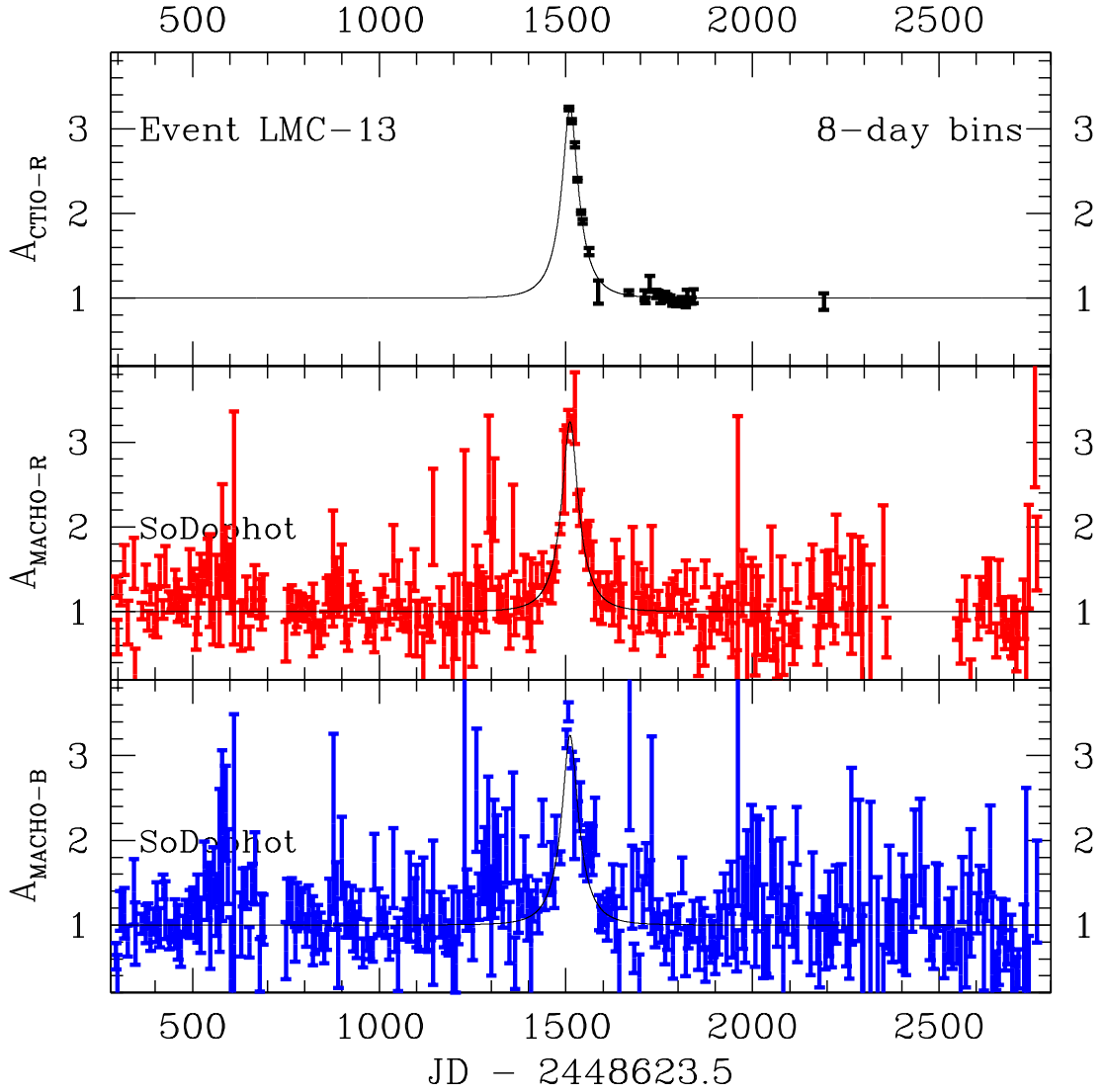


Fig. 4.— The MACHO and GMAN-CTIO (top panel) follow-up data are shown in the full light curve for microlensing event LMC-13 (also known as MACHO-96-LMC-1). The solid line is the best fit light curve constrained to match the HST V-band magnitude, and all data is presented in 8-day bins.

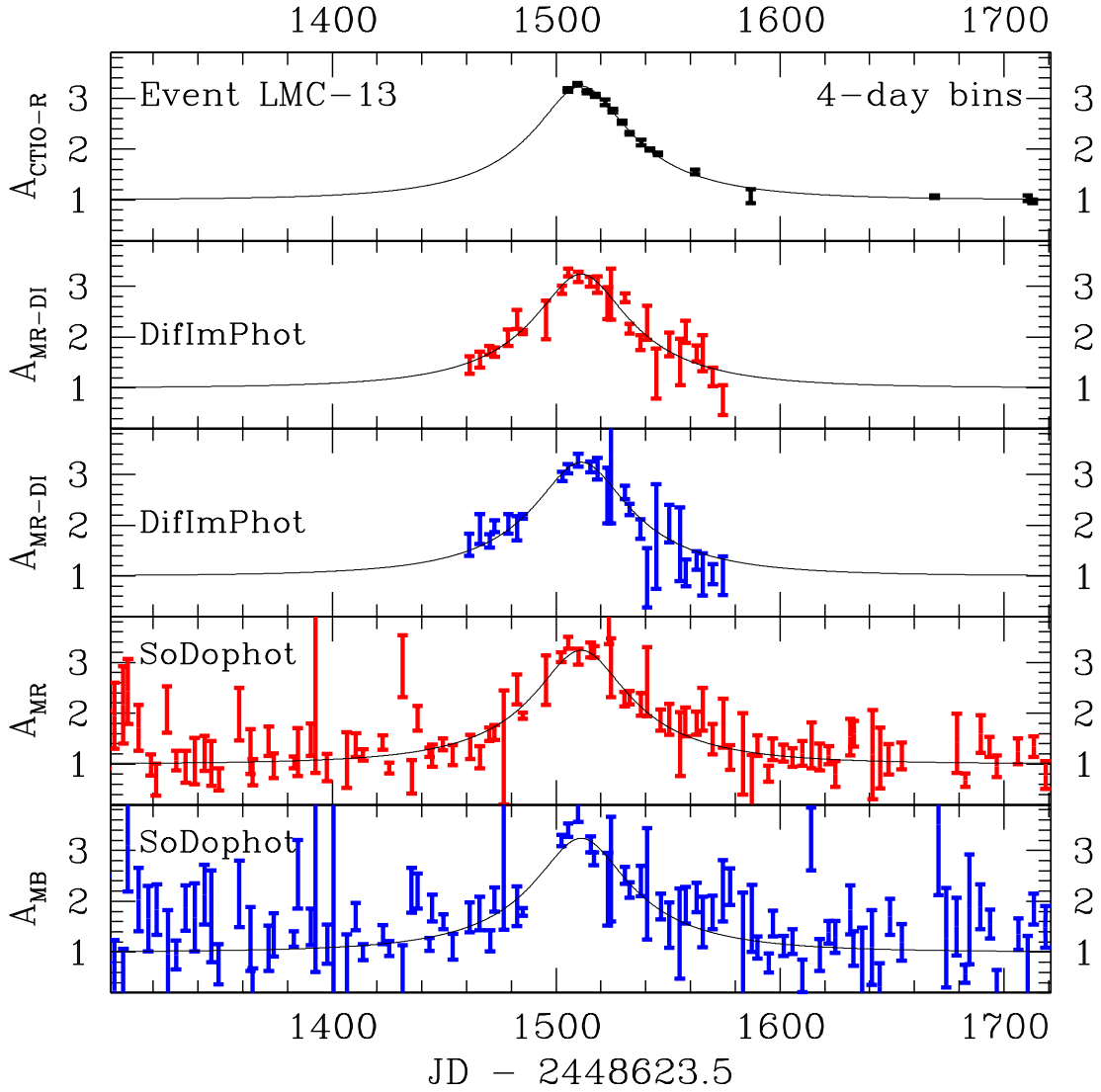


Fig. 5.— The MACHO and GMAN-CTIO (top panel) follow-up data are shown in a close-up of the light curve for microlensing event LMC-13. All data is presented in 4-day bins, and the 2-band MACHO data is presented with the original SoDophot photometry (bottom 2 panels) as well as photometry from the DifImPhot package. For this event, the photometric noise has been substantially reduced by the DifImPhot photometry.

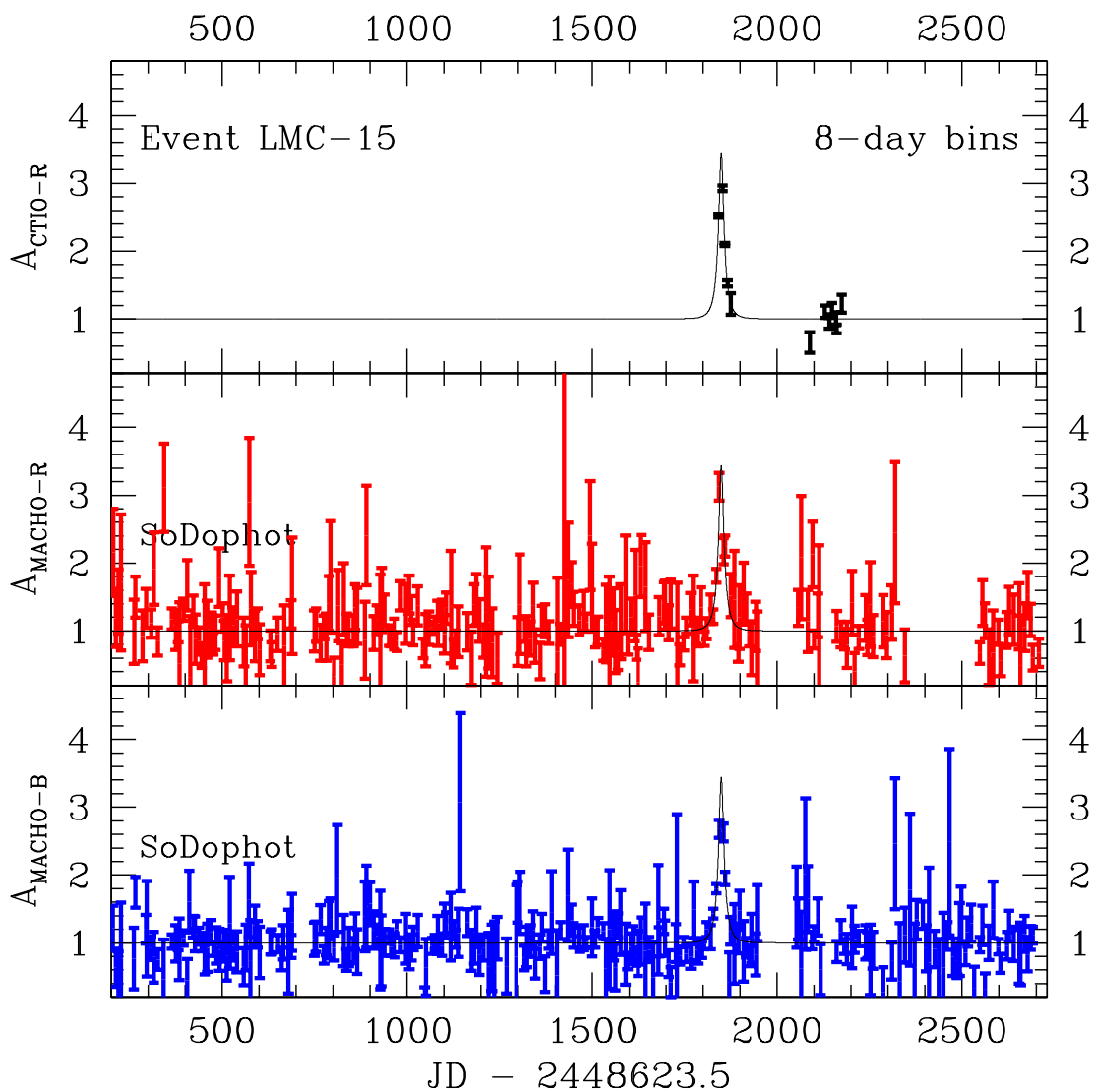


Fig. 6.— The MACHO and GMAN-CTIO (top panel) follow-up data are shown in the full light curve for microlensing event LMC-15 (also known as MACHO-97-LMC-1). The solid line is the best fit light curve constrained to match the HST V-band magnitude, and all data is presented in 8-day bins.

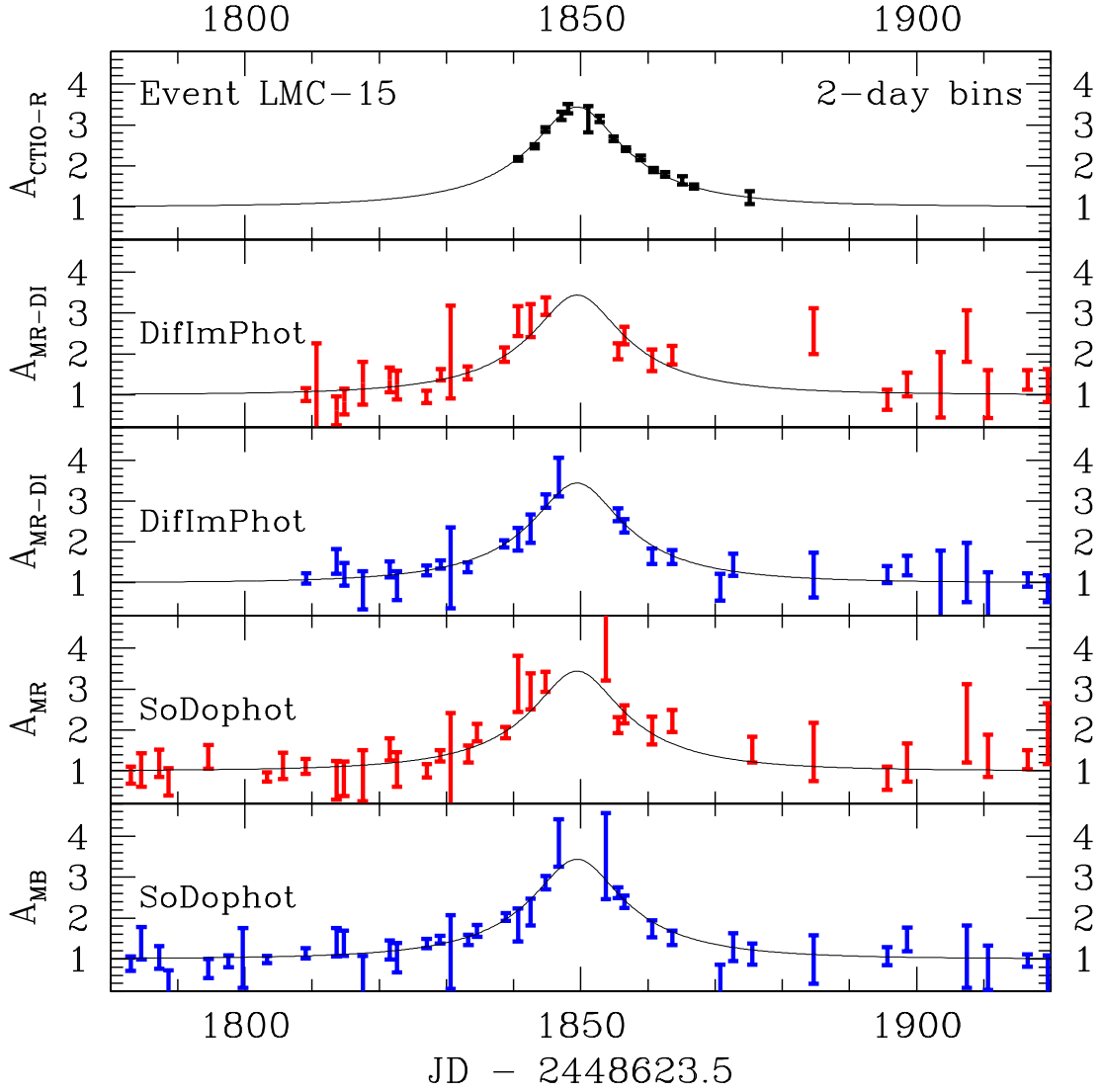


Fig. 7.— The MACHO and GMAN-CTIO (top panel) follow-up data are shown in a close-up of the light curve for microlensing event LMC-15. All data is presented in 2-day bins, and the 2-band MACHO data is presented with the original SoDophot photometry (bottom 2 panels) as well as photometry from the DifImPhot package.

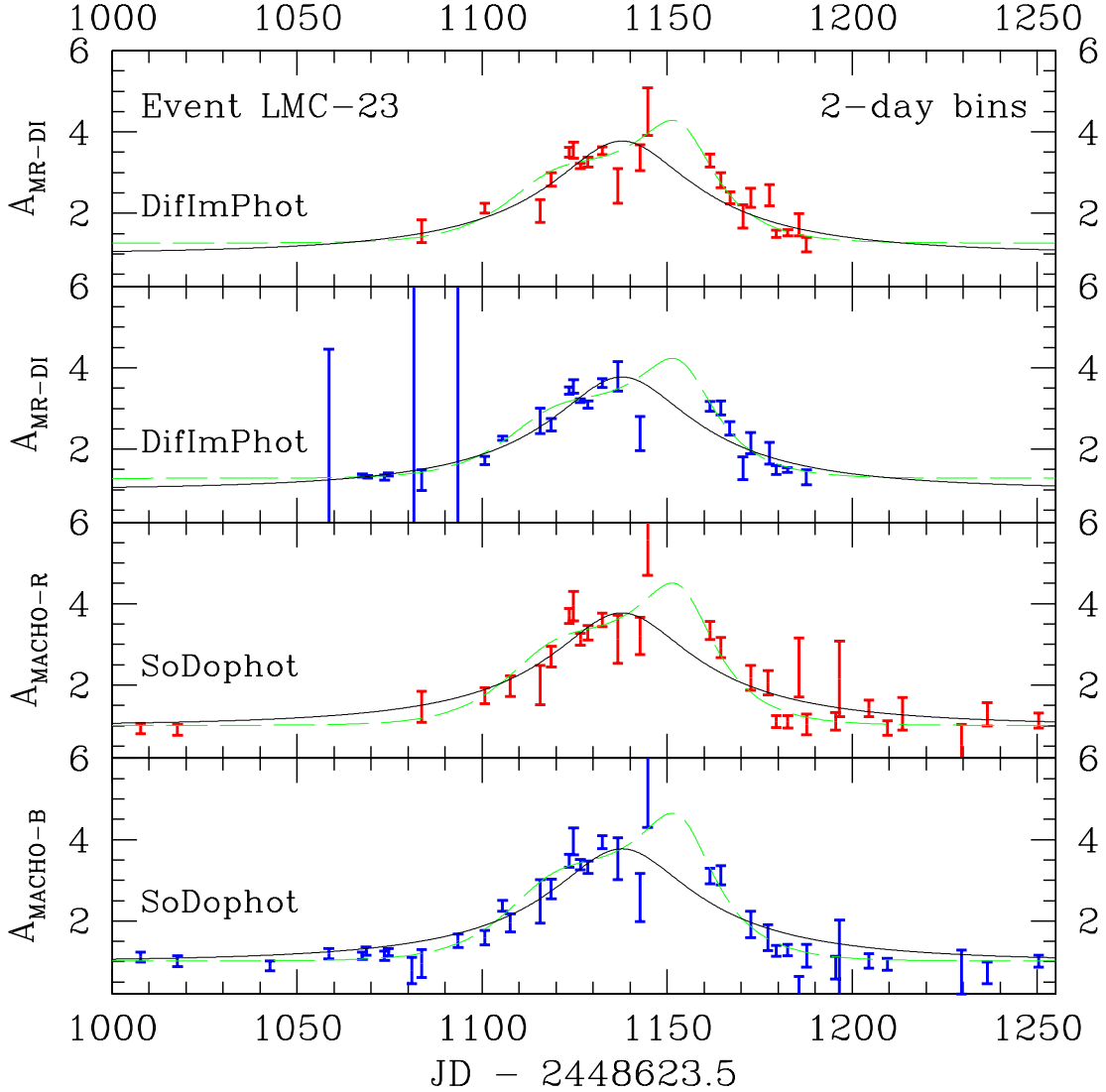


Fig. 8.— The MACHO data are shown in a close-up of the light curve of pseudo-microlensing event LMC-23, which has recently been observed to have a 2nd brightening episode which makes the microlensing interpretation extremely unlikely. The data is presented in 2-day bins, with both the original SoDophot photometry (bottom 2 panels) as well as photometry from the DifImPhot package. The dashed green curve is a microlensing parallax fit, which provides a substantially better fit to the data (but is also unlikely to be correct).

Table 1. Microlensing Fit Parameters

Event	f_{MR}	f_{MB}	f_{CTIO}	$V_M \equiv V_{HST}$	R_M	R_{HST}	t_0 (MJD)	u_0	t_E (days)	$\frac{\chi^2}{(\text{dof})}$
LMC-4	0.384(7)	0.335	0.598(16)	21.33(3)	21.15(6)	21.09(3)	1022.86(6)	0.147(2)	39.5(7)	1.418
LMC-13	0.66(2)	0.564	0.77(2)	21.76(3)	21.38(6)	21.38(3)	1511.2(2)	0.320(7)	66.0(1.3)	1.177
LMC-15	0.73(6)	0.755	0.65(3)	21.18(3)	21.10(9)	21.07(3)	1849.4(1)	0.300(12)	22(1)	0.979
<i>LMC-23</i>	0.42(2)	0.508	–	21.05(3)	<i>20.92(6)</i>	20.64(3)	1137.8(5)	0.272(8)	70(2)	1.730
<i>LMC-23-p</i>	0.40(2)	0.508	–	21.05(3)	<i>20.95(6)</i>	20.64(3)	1135.8(4)	–2.48(16)	16.2(8)	1.410

Note. — The columns of this table list the fit parameters for each event. f_{MR} , f_{MB} , and f_{CTIO} are the blend fractions for the MACHO red and blue, and CTIO data sets. V_M , R_M , V_{HST} , and R_{HST} are the calibrated V and R band source star brightnesses for the MACHO (Alcock et al. 1999a) and HST photometry. t_0 , u_0 and t_E are the standard Paczyński microlensing light curve fit parameters. t_0 and u_0 are the time of peak magnification and the impact parameter, given in units of the Einstein ring radius. t_E is the Einstein radius crossing time.

Table 2. Microlensing Fit χ^2 Values

Event		MACHO-R		MACHO-R-DI		MACHO-B		MACHO-B-DI		CTIO-R	
		N_{data}	$\frac{\chi^2}{(\text{dof})}$	N_{data}	$\frac{\chi^2}{(\text{dof})}$	N_{data}	$\frac{\chi^2}{(\text{dof})}$	N_{data}	$\frac{\chi^2}{(\text{dof})}$	N_{data}	$\frac{\chi^2}{(\text{dof})}$
LMC-4	full	730	1.368	85	1.355	728	1.522	78	1.742	134	0.989
	peak	92	1.573	85	1.355	91	1.430	78	1.742	107	1.072
LMC-13	full	1074	1.256	84	1.376	1176	1.196	84	1.026	332	0.937
	peak	165	1.056	84	1.376	171	1.557	84	1.026	182	0.925
LMC-15	full	475	0.984	47	1.272	586	0.914	49	1.067	60	1.303
	peak	29	1.144	25	1.607	32	0.752	28	0.694	39	0.876
<i>LMC-23</i>	full	389	1.498	24	4.846	382	1.495	30	5.814	0	–
	peak	31	3.413	24	4.846	41	3.229	30	5.814	0	–
<i>LMC-23-p</i>	full	389	1.364	24	2.434	382	1.284	30	3.012	0	–
	peak	31	1.688	24	2.434	41	1.310	30	3.012	0	–

Table 3. $\Delta\chi^2$ Values

Event	MACHO-R	MACHO-R-DI	MACHO-B	MACHO-B-DI	CTIO-R	CTIO-B	total
LMC-4	5540.5	11664.2	5977.4	11687.8	4621.3	–	27973.3
LMC-13	2037.0	2377.6	1419.2	1543.8	17523.1	–	21444.5
LMC-14	5229.8	6328.6	10860.0	13868.0	69274.8	64081.7	153553.0
LMC-15	254.3	234.2	554.0	437.8	2204.0	–	3012.2

Table 4. Event Classification

Event	MACHO Verdict	BEL Verdict	confirmation	Mancini et al lens type
1	μ lens-A	μ lens	clump giant	non-LMC
4	μ lens-A	variable	CTIO+DIP phot.	non-LMC
5	μ lens-A	μ lens	lens ID	MW-disk
6	μ lens-A	μ lens	–	LMC
7	μ lens-A	variable	–	non-LMC
8	μ lens-A	variable	–	LMC
9	μ lens-B	–	caustic-binary	LMC
10	SN	μ lens	<i>HST: galaxy</i>	–
11	SN	SN	<i>HST: galaxy</i>	–
12	SN	SN	<i>HST: galaxy</i>	–
13	μ lens-A	variable	CTIO+DIP phot.	LMC
14	μ lens-A	μ lens	CTIO+DIP phot.	LMC
15	μ lens-A	variable	CTIO+DIP phot.	non-LMC
16	SN	–	<i>CTIO: galaxy</i>	–
17	SN	SN	<i>CTIO: galaxy</i>	–
18	μ lens-A	variable	–	non-LMC
19	SN	SN	<i>CTIO: galaxy</i>	–
20	μ lens-B	SN	–	–
21	μ lens-A	μ lens	–	non-LMC
22	B	μ lens	<i>MSSSO: galaxy</i>	–
23	μ lens-A	μ lens	<i>variable</i>	–
24	SN	μ lens	<i>MACHO: galaxy</i>	–
25	μ lens-A	μ lens	clump giant	non-LMC
26	SN	variable	–	–
27	μ lens-B	variable	–	–

Note. — The event classification results of MACHO and BEL are compared to the results of additional data that can confirm or reject each event. Confirmed microlensing events have bold face entries in the confirmation column, and rejected microlensing candidates have entries in italics